Article:
Douverne, M, Ning, Y, Tatani, A et al. (2 more authors) (2019) How Many Phosphoric Acid Units Are Required to Ensure Uniform Occlusion of Sterically Stabilized Nanoparticles within Calcite? Angewandte Chemie - International Edition, 58 (26). pp. 8692-8697. ISSN 1433-7851

https://doi.org/10.1002/anie.201901307

How Many Phosphoric Acid Units Are Required to Ensure Uniform Occlusion of Sterically-Stabilized Nanoparticles within Calcite?

Marcel Douverne,[a,b] Yin Ning,[*,a] Aikaterini Tatani,[a] Fiona C. Meldrum[c] and Steven P. Armes[*,a]

[a] M. Douverne, Dr. Y. Ning, A. Tatani, and Prof. S. P. Armes
Department of Chemistry, University of Sheffield, Brook Hill, Sheffield, South Yorkshire S3 7HF, U.K.
E-mail: Y.Ning@sheffield.ac.uk; s.p.armes@sheffield.ac.uk

[b] M. Douverne
Faculty of Chemistry, Pharmaceutical Sciences and Geosciences, Johannes Gutenberg-University Mainz, Duesbergweg 10-14, 55128 Mainz, Germany.

[c] Prof. F. C. Meldrum
School of Chemistry, University of Leeds, Woodhouse Lane, Leeds, LS2 9JT, U.K.

Abstract: Polymerization-induced self-assembly (PISA) mediated by reversible addition-fragmentation chain transfer (RAFT) polymerization offers a platform technology for the efficient and versatile synthesis of well-defined sterically-stabilized block copolymer nanoparticles. Herein we synthesize a series of such nanoparticles with tunable anionic charge density within the stabilizer chains, which are prepared via statistical copolymerization of anionic 2-(phosphonooxy)ethyl methacrylate (P) with non-ionic glycerol monomethacrylate (G). Systematic variation of the P/G molar ratio enables elucidation of the *minimum* number of phosphate groups per copolymer chain required to promote nanoparticle occlusion within a model inorganic crystal (calcite). Moreover, the extent of nanoparticle occlusion correlates strongly with the phosphate content of the steric stabilizer chains. This study is the first to examine the effect of systemically varying the anionic charge density of nanoparticles on their occlusion efficiency and sheds new light on maximizing guest nanoparticles loading within calcite host crystals.

Polymerization-induced self-assembly (PISA) has been the subject of considerable recent attention because it provides a powerful route for the synthesis of well-defined block copolymer nano-objects (e.g., spheres, worms or vesicles, etc.) at remarkably high copolymer concentration.[1] This technique usually involves reversible addition-fragmentation chain transfer (RAFT) polymerization and is applicable to a wide range of functional monomers.[2] PISA has been intensively explored by many research groups within the past decade.[3] In principle, phosphorus-based polymers offer enormous potential biomedical applications owing to their excellent biocompatibility[4] and strong affinity for biominerials (e.g., hydroxyapatite[5]). Vinylphosphonic acid (VPA) was the first reported *anionic* phosphorus monomer to be polymerized directly via controlled radical polymerization by Destarac and co-workers.[6] However, the direct PISA synthesis of phosphorus-based copolymer *nanoparticles* is rather rare. Both Monge[7] and Hanisch[8] reported the *indirect* RAFT synthesis of poly(methacryloyloxymethyl phosphonic acid) (PMPA) by hydrolysis of a poly(dimethyl(methacryloyloxy)methyl phosphonate) precursor. Moreover, Hanisch and co-workers explored the PISA synthesis of sterically-stabilized diblock copolymer nanoparticles via chain

extension of a PMPA precursor using benzyl methacrylate. After deprotection to confer anionic character, the occlusion of such diblock copolymer nanoparticles within calcite crystals was also

briefly studied.[8] However, scanning electron microscopy (SEM) studies revealed that such nanoparticles were merely surface-confined, rather than uniformly distributed throughout the calcite crystals.

Crystallization normally involves the expulsion of impurities rather than their incorporation. Thus nanoparticle occlusion within growing crystal hosts is somewhat counter-intuitive.[9] Nevertheless, a growing number of studies have demonstrated nanoparticle occlusion within various inorganic crystals, including Cu_2O, $CaCO_3$, ZnO and $CaSO_4{\cdot}0.5H_2O$.[10] This strategy provides a straightforward route to prepare hybrid nanocomposite crystals. In at least some cases (e.g. calcite), it also enhances our understanding of biomineralization.[11]

The efficient occlusion of sterically-stabilized nanoparticles is typically achieved using an anionic steric stabilizer.[10c, 12] Herein, we employ RAFT polymerization to statistically copolymerize two commercially available monomers, 2-(phosphonooxy)ethyl methacrylate (bearing *phosphoric acid* groups, denoted as P) and glycerol monomethacrylate (*non-ionic*, denoted as G) in methanol, see **Scheme 1**. Subsequent chain extension of this statistical copolymer with a suitable hydrophobic core-forming monomer, benzyl methacrylate (B), produces well-defined spherical nanoparticles. For brevity, poly(2-(phosphonooxy)ethyl methacrylate-*stat*-glycerol monomethacrylate)-poly(benzyl methacrylate) is denoted as (P-*stat*-G)-B. The P/G molar ratio was systematically varied to adjust the phosphoric acid content within the steric stabilizer chains of the resulting copolymer nanoparticles. These model nanoparticles enable us to address the following important question in nanoparticle occlusion studies: *what is the minimum number of anionic comonomer units in the steric stabilizer block that is required to achieve uniform nanoparticle occlusion within calcite crystals?*

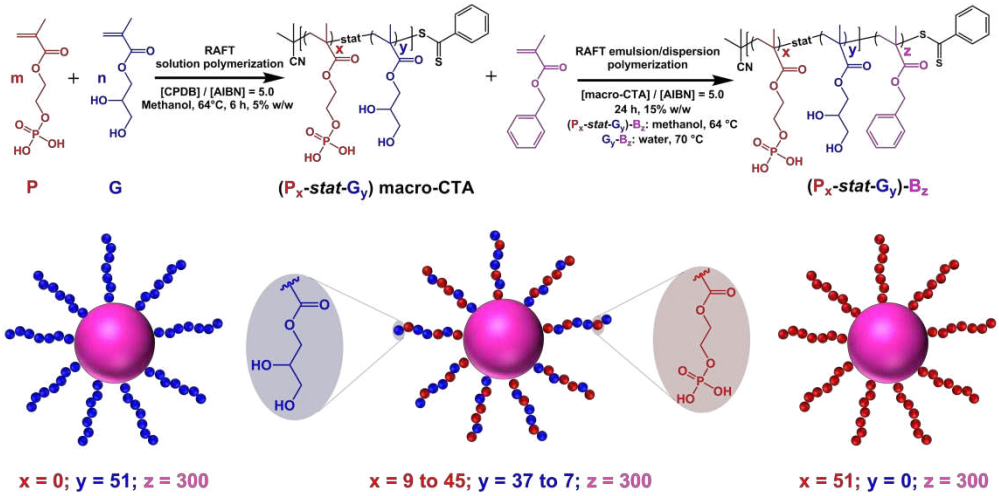

Scheme 1. The two-step synthesis of poly(2-(phosphonooxy)ethyl methacrylate-*stat*-glycerol monomethacrylate)-poly(benzyl methacrylate) [(P-*stat*-G)-B] copolymer nanoparticles in methanol was achieved by (i) statistical copolymerization of 2-(phosphonooxy)ethyl methacrylate (P) and glycerol monomethacrylate (G) via reversible addition-fragmentation chain transfer (RAFT) solution polymerization at 5% w/w solids and (ii) RAFT dispersion polymerization of benzyl methacrylate (B) at 15% w/w solids. [N.B. A relatively dilute solution was deliberately chosen in the case of (i) in order

to minimize branching/crosslinking owing to the relatively high level of dimethacrylate impurity present in the P comonomer]. Judicious variation of the P/G molar ratio enables preparation of a series of sterically-stabilized nanoparticles with tunable anionic charge density. The corresponding schematic cartoons illustrate the three types of sterically-stabilized nanoparticles that can be targeted by this approach, which comprise either zero, intermediate or maximum (100%) content of the anionic phosphate comonomer. It is noted that colloidal stable G_{51}-B_{300} nanoparticles were prepared via RAFT aqueous emulsion polymerization while the rest were made by RAFT dispersion polymerization in methanol.

A series of macromolecular chain transfer agents (macro-CTAs) were synthesized by statistically copolymerizing the anionic P monomer and non-ionic G monomer using various molar ratios to tune the anionic content of this steric stabilizer block (see **Scheme 1** and Supporting Information). The corresponding fully anionic and wholly non-ionic homopolymer macro-CTAs were also prepared. ^{1}H NMR spectroscopy studies indicated that, on increasing the P/G molar ratio, the signal assigned to pendent protons on the P comonomer systematically increase in relative intensity compared to those assigned to the pendent protons on the G residues (see **Figure S1**). Aqueous gel permeation chromatography (GPC) studies confirmed that a unimodal curve for each macro-CTA but relatively high dispersities ($1.34 < M_w/M_n < 1.54$). However, the latter data are most likely the result of an unfavourable interaction between the G comonomer units in the copolymer chains with the aqueous GPC columns, which leads to low molecular weight tailing and hence broader *apparent* dispersity. This hypothesis is supported by the following observations: GPC analysis of a G_{51} homopolymer using DMF eluent indicated a number-average molecular weight (M_n) of 12.9 kg mol^{-1} and an M_w/M_n of 1.18 (**Figure S2a**), while analysis of the same homopolymer by aqueous GPC yielded a much lower molecular weight and a significantly broader molecular weight distribution (M_n = 1.2 kg mol^{-1} and an M_w/M_n of 1.54) (**Figure S2b**). The latter data set is clearly consistent with unfavourable interactions between this G_{51} homopolymer and the GPC columns. In principle, this analytical problem should be weaker for the statistical copolymers because of their lower G content. Indeed, this appears to be the case: higher dispersities are observed for G-rich copolymers (**Figure S2**).

These macro-CTAs were subsequently chain-extended with water-insoluble benzyl methacrylate targeting a fixed core-forming block DP of 300 via RAFT-mediated PISA. Uniform copolymer nanoparticles were obtained, as judged by electron microscopy studies (see **Figures 1a-1f**). Such nanoparticles contain from 0 to 51 anionic phosphate groups within each steric stabilizer chain. Dynamic light scattering (DLS) studies indicated that the mean hydrodynamic diameter of these nanoparticles ranges from ~90 nm to ~140 nm (see **Table S1**). The relatively small size obtained for the G_{51}-B_{300} nanoparticles is attributed to the RAFT aqueous emulsion polymerization formulation used for this PISA synthesis. Such size differences are not expected to significantly affect their extent of occlusion. Indeed, previous studies suggest that nanoparticles ranging from 20 nm to 200 nm can be efficiently occluded within calcite.[10f, 12d] The nanoparticle density increases monotonically with anionic phosphate content (**Table S1**) as determined by helium pycnometry at 20 °C. Moreover, aqueous electrophoresis studies conducted in the absence of any Ca^{2+} confirmed that nanoparticle zeta potentials vary according to their anionic phosphate content, with a higher proportion of phosphate comonomer leading to a more negative zeta potential (see **Figure 1g** and **Table S1**). As expected, the presence of Ca^{2+} ions has no discernible effect on the electrophoretic behavior of the

non-ionic G_{51}-B_{300} nanoparticles, which are only very weakly anionic. However, zeta potentials for nanoparticles containing anionic phosphate groups in their steric stabilizer chains are significantly lowered in the presence of Ca^{2+} ions, which indicates cation binding (**Figure 1h**).

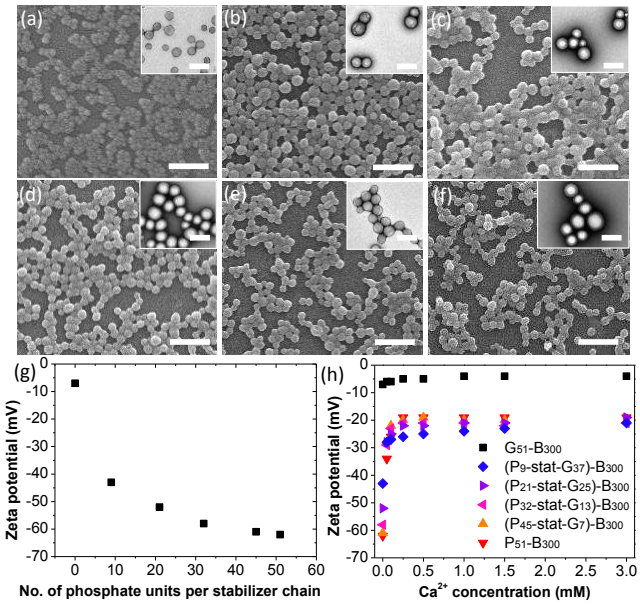

Figure 1. SEM images (insets are corresponding TEM images) and aqueous electrophoresis data recorded for a series of diblock copolymer nanoparticles containing variable amounts of phosphate comonomer with the steric stabilizer block: (a) G_{51}-B_{300}; (b) (P_9-*stat*-G_{37})-B_{300}; (c) (P_{21}-*stat*-G_{25})-B_{300}; (d) (P_{32}-*stat*-G_{13})-B_{300}; (e) (P_{45}-*stat*-G_7)-B_{300}; (f) P_{51}-B_{300}. (g) Zeta potential vs. number of phosphate units per stabilizer chain in the absence of Ca^{2+} ions, indicating more negative zeta potentials being observed as the proportion of anionic phosphate groups per stabilizer chain is increased. (h) Variation of zeta potential with Ca^{2+} concentration for each of these six types of nanoparticles. The scale bars in the SEM images correspond to 500 nm while the scale bars in the inset TEM images correspond to 200 nm.

Calcium carbonate ($CaCO_3$) crystals were formed at around pH 9 by exposing an aqueous solution containing 1.0 mM Ca^{2+} and 0.10% w/w nanoparticles to ammonium carbonate vapor at 20 °C for 24 h.[13] Negligible occlusion was observed when G_{51}-B_{300} nanoparticles were employed under these conditions (**Figure 2a** and **Figure S3**). In contrast, *non-uniform* occlusion was observed for (P_9-*stat*-G_{37})-B_{300} nanoparticles and (P_{21}-*stat*-G_{25})-B_{300} copolymer nanoparticles (**Figures 2b** and **2c**; **Figures S4** and **S5**). The former copolymer nanoparticles were preferentially located at the near surface of the crystals (see **Figure S4**). A further increase in anionic phosphate content led to uniform occlusion of the (P_{32}-*stat*-G_{13})-B_{300} nanoparticles throughout the whole crystals (**Figure 2d** and **Figure S6**). Moreover, using anionic phosphate-rich sterically-stabilized nanoparticles such as (P_{45}-*stat*-G_7)-B_{300} and P_{51}-B_{300} leads to relatively high, uniform occlusion (**Figures 2e** and **2f**; **Figures S7** and **S8**).

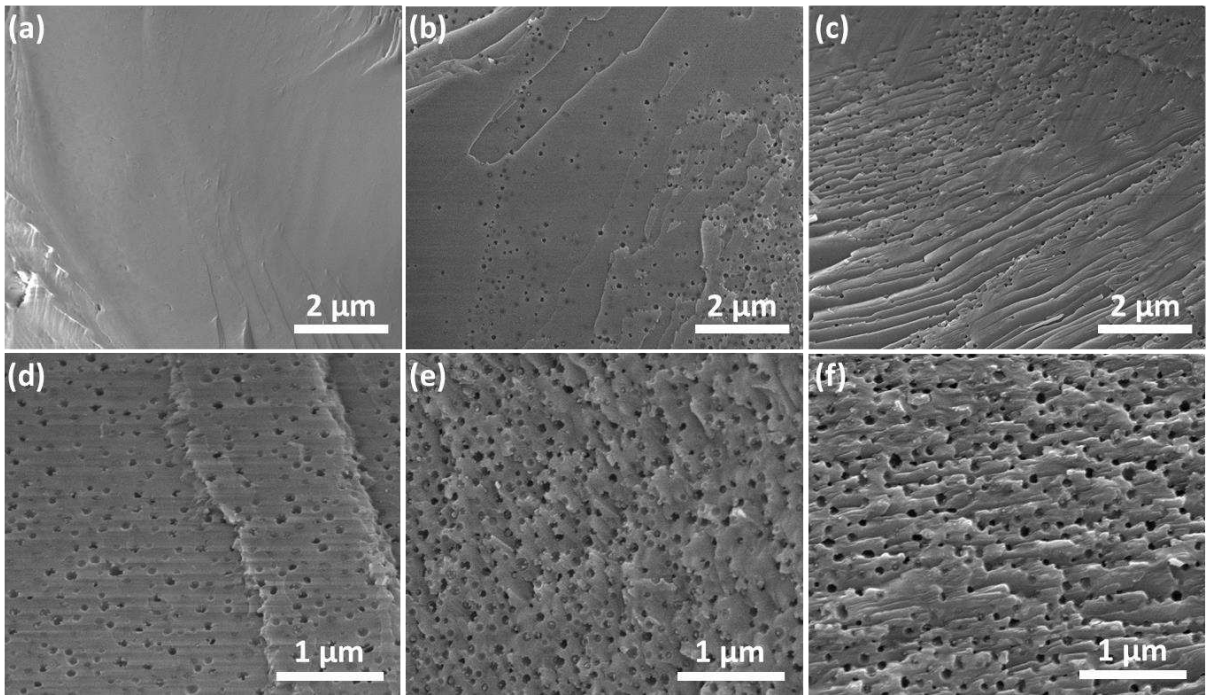

Figure 2. SEM images recorded for randomly-fractured $CaCO_3$ crystals prepared in the presence of 0.1% w/w sterically-stabilized nanoparticles plus 1.0 mM $CaCl_2$ at 20 °C for 24 h. (a) G_{51}-B_{300}; (b) (P_9-*stat*-G_{37})-B_{300}; (c) (P_{21}-*stat*-G_{25})-B_{300}; (d) (P_{32}-*stat*-G_{13})-B_{300}; (e) (P_{45}-*stat*-G_7)-B_{300}; (f) P_{51}-B_{300}.

Raman spectroscopy studies confirmed that the polymorph of these $CaCO_3$ crystals is invariably calcite, with characteristic bands being observed at 1088 cm^{-1} (v_1), 712 cm^{-1} (v_4), 281 cm^{-1} and 154 cm^{-1} (lattice modes) (see **Figure S9**).[14] The extent of nanoparticle occlusion increases systematically for higher anionic phosphate contents and the extent of occlusion by volume can be calculated from thermogravimetric analysis (see **Figures 3a** and **3b**). Given that the nanoparticles in this study are relatively uniform in size, the mean inter-particle distance can be estimated using the following equation (detailed mathematical calculations are given in the supporting information):

$$d = 2r\left(\sqrt[3]{\frac{p}{E}} - 1\right)$$

where *r*, *E* and *p* are the nanoparticle radius, the extent of occlusion by volume and the nanoparticle packing efficiency (for random packing, $p = 0.64$[15]), respectively.

Figure 3c shows that the inter-particle distance is systematically reduced for higher anionic phosphate contents, indicating higher extents of occlusion. This finding is in good agreement with the corresponding SEM observations (see **Figure 2**).

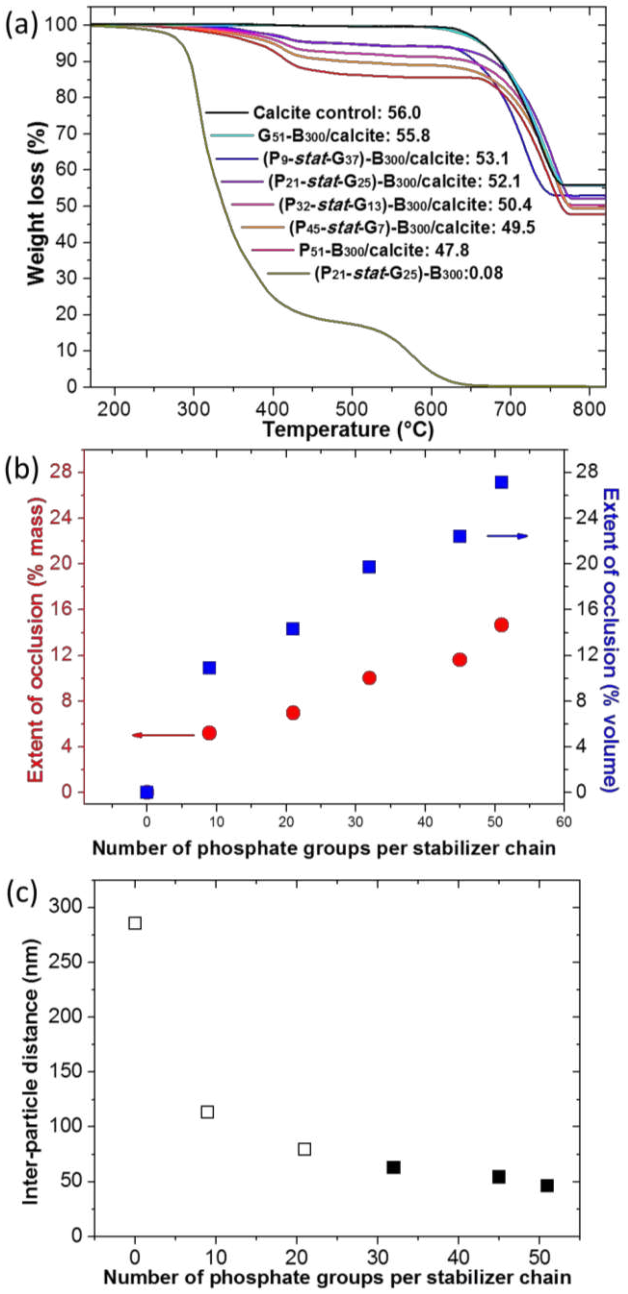

Figure 3. (a) Thermogravimetric analysis curves recorded for various diblock copolymer nanoparticles, the corresponding copolymer nanoparticle/calcite nanocomposite crystals and a calcite control. (b) Extent of nanoparticle occlusion (by mass and by volume) vs. number of phosphate repeat units per copolymer chain. (c) Inter-particle distance as a function of number of anionic phosphate groups per stabilizer chain. [N.B. The empty squares are calculated by assuming that the nanoparticles are uniformly occluded within calcite. In fact, only the filled squares correspond to uniform nanoparticle occlusion.]

The main aim of this study was to examine how the number of anionic phosphate units on the steric stabilizer influences the extent of nanoparticle occlusion within calcite for an approximately constant stabilizer DP. We have not attempted to vary the stabilizer DP in the present study. This is because

we have recently shown that using relatively long anionic stabilizer chains does not promote nanoparticle occlusion but instead results in a significant change in the crystal morphology.[16] In principle, a series of P_x-B_{300} diblock copolymer nanoparticles of varying x could be readily synthesized via RAFT dispersion polymerization. However, using shorter stabilizer chains (e.g. DP = 25) for such PISA syntheses would lead to significantly larger nanoparticles with relatively high stabilizer surface densities. On the other hand, longer stabilizer chains (e.g. DP = 100) should result in smaller nanoparticles with relatively low stabilizer surface densities.[12d] More importantly, a relatively short stabilizer chain DP is expected to restrict the conformational entropy of the stabilizer chains,[17] hence reducing nanoparticle binding to the growing crystal surface and thus reducing nanoparticle occlusion.[18] Conveniently, statistical copolymerization of the non-ionic G monomer with the anionic P monomer while targeting a constant intermediate DP of around 50 can avoid the problems mentioned above. Prior study showed P_{32}-B_{300} nanoparticles are surface-confined[18] whilst (P_{32}-*stat*-G_{13})-B_{300} are uniformly occluded. This is most probably because the latter can adopt more possible conformations.

Nanoparticle occlusion within inorganic crystals is a complex process that is influenced by many parameters.[10e, 12b-d] Liu and co-workers reported that nanoparticles can be passively incorporated into calcite using a gel-trapping method.[19] In this case, there is no specific requirement for the nanoparticle surface chemistry provided that they can be physically entrapped within an appropriate gel network. However, for *active* nanoparticle occlusion within growing inorganic crystals, the nanoparticle surface chemistry dictates whether occlusion occurs and also to what extent.[10e, 12b] In the present study, nanoparticles with low phosphate content are preferentially occluded within the near-surface of the calcite crystals (see **Figure 2b** and **Figure S4**), because there are insufficient anionic groups to ensure adequate binding to the growing crystal surface. Such surface-confined occlusion suggests that nanoparticle occlusion only occurs at the latter stages, where the rate of calcite growth and calcium ions both are reduced. However, both step lengths and kink sites are more prevalent under these conditions, which facilitates nanoparticle occlusion.[18] More uniform, dense nanoparticle occlusion can be achieved at higher anionic phosphate contents (see **Figures 2d~2f**). This is because there are now sufficient anionic groups to ensure strong binding to the crystal surface, which leads to nanoparticle engulfment by the advancing steps. $CaCO_3$ crystals precipitated in the presence of an equivalent *molar* concentration of each of the water-soluble macro-CTAs used in this study (e.g. G_{51}, P_{51} and P_{32}-*stat*-G_y) exhibit significant differences in morphology. For non-ionic G_{51}, perfect rhombohedral $CaCO_3$ crystals were obtained, suggesting that G_{51} does not affect crystal growth. In contrast, flower-like crystals were observed when $CaCO_3$ was precipitated in the presence of (P_{32}-*stat*-G_{13}), (P_{45}-*stat*-G_7) or P_{51}. This indicates a relatively strong interaction between the inorganic and organic components when using phosphate-rich anionic copolymer chains (see **Figure S10**).

In summary, a series of phosphate-based diblock copolymer nanoparticles with narrow size distributions and varying phosphate content has been conveniently prepared by RAFT-mediated PISA. Precipitation of calcite crystals in the presence of these model copolymer nanoparticles confirmed that a relatively low proportion of anionic phosphate groups (e.g. < 21 phosphate groups per stabilizer chain) led to non-uniform occlusion (e.g. surface-confined occlusion) while a relatively high proportion (e.g. 32 phosphate groups per stabilizer chain) ensured efficient uniform occlusion. In summary, this study provides important guidelines for the rational design of sterically-stabilized

nanoparticles to enable their efficient occlusion within host crystals, which is an attractive route to novel hybrid nanocomposites.

Acknowledgements

EPSRC (EP/P005241/1) is thanked for post-doctoral support for Y.N. and S.P.A. also acknowledges an EPSRC Established Career Particle Technology Fellowship (EP/R003009/1). F.C.M. thanks the EPSRC for support under project EP/P005233/1.

Author Contributions

Y.N. and S.P.A. led the project. M.D. and A.T. synthesized the (co)polymers and grew the calcite crystals under the supervision of Y.N. Y.N. characterized the samples and analyzed the data. Y.N. and S.P.A. co-wrote the manuscript and F.C.M commented on it.

Keywords: polymerization-induced self-assembly • RAFT polymerization • block copolymer self-assembly • nanoparticle occlusion • calcite.

References

[1] a) J.-T. Sun, C.-Y. Hong, C.-Y. Pan, *Polym. Chem.* **2013**, *4*, 873-881; b) N. J. Warren, S. P. Armes, *J. Am. Chem. Soc.* **2014**, *136*, 10174-10185; c) A. B. Lowe, *Polymer* **2016**, *106*, 161-181; d) M. J. Derry, L. A. Fielding, S. P. Armes, *Prog. Polym. Sci.* **2016**, *52*, 1-18; e) S.-L. Chen, P.-F. Shi, W.-Q. Zhang, *Chin. J. Polym. Sci.* **2017**, *35*, 455-479; f) S. Y. Khor, J. F. Quinn, M. R. Whittaker, N. P. Truong, T. P. Davis, *Macromol. Rapid Commun.* **2018**, 1800438.
[2] a) X. Wang, Z. An, *Macromol. Rapid Commun.* **2019**, *40*, 1800325; b) D. Le, D. Keller, G. Delaittre, *Macromol. Rapid Commun.* **2018**, 1800551; c) S. L. Canning, G. N. Smith, S. P. Armes, *Macromolecules* **2016**, *49*, 1985-2001; d) J. Yeow, C. Boyer, *Adv. Sci.* **2017**, *4*, 1700137; e) M. Huo, D. Li, G. Song, J. Zhang, D. Wu, Y. Wei, J. Yuan, *Macromol. Rapid Commun.* **2018**, *39*, 1700840; f) L. Zhang, Q. Lu, X. Lv, L. Shen, B. Zhang, Z. An, *Macromolecules* **2017**, *50*, 2165-2174.
[3] a) Y. Li, S. P. Armes, *Angew. Chem. Int. Ed.* **2010**, *49*, 4042-4046; b) J. Tan, H. Sun, M. Yu, B. S. Sumerlin, L. Zhang, *ACS Macro Lett.* **2015**, *4*, 1249-1253; c) D. Zhou, S. Dong, R. P. Kuchel, S. Perrier, P. B. Zetterlund, *Polym. Chem.* **2017**, *8*, 3082-3089; d) C. E. Boott, J. Gwyther, R. L. Harniman, D. W. Hayward, I. Manners, *Nat. Chem.* **2017**, *9*, 785; e) N. J. Penfold, Y. Ning, P. Verstraete, J. Smets, S. P. Armes, *Chem. Sci.* **2016**, *7*, 6894-6904; f) J. Lesage de la Haye, X. Zhang, I. Chaduc, F. Brunel, M. Lansalot, F. D'Agosto, *Angew. Chem. Int. Ed.* **2016**, *55*, 3739-3743; g) R. Deng, M. J. Derry, C. J. Mable, Y. Ning, S. P. Armes, *J. Am. Chem. Soc.* **2017**, *139*, 7616-7623; h) L. D. Blackman, S. Varlas, M. C. Arno, Z. H. Houston, N. L. Fletcher, K. J. Thurecht, M. Hasan, M. I. Gibson, R. K. O'Reilly, *ACS Centr. Sci.* **2018**, *4*, 718-723; i) Y. Ding, M. Cai, Z. Cui, L. Huang, L. Wang, X. Lu, Y. Cai, *Angew. Chem. Int. Ed.* **2018**, *57*, 1053–1056; j) H. Yao, Y. Ning, C. P. Jesson, J. He, R. Deng, W. Tian, S. P. Armes, *ACS Macro Lett.* **2017**, *6*, 1379-1385; k) J. Foster, S. Varlas, B. Couturaud, J. Jones, R. Keogh, R. Mathers, R. K. O'Reilly, *Angew. Chem. Int. Ed.* **2018**; l) G. Mellot, J.-M. Guigner, L. Bouteiller, F. Stoffelbach, J. Rieger, *Angew. Chem.* **2019**, *131*, 3205-3209.
[4] a) Z. Lin, S. Cao, X. Chen, W. Wu, J. Li, *Biomacromolecules* **2013**, *14*, 2206-2214; b) S. Monge, B. Canniccioni, A. Graillot, J.-J. Robin, *Biomacromolecules* **2011**, *12*, 1973-1982; c) J. Z. Du, Y. Q. Tang, A. L. Lewis, S. P. Armes, *J. Am. Chem. Soc.* **2005**, *127*, 17982-17983; d) J. Madsen, I. Canton, N. J. Warren, E. Themistou, A. Blanazs, B. Ustbas, X. Tian, R. Pearson, G. Battaglia, A. L. Lewis, S. P. Armes, *J. Am. Chem. Soc.* **2013**, *135*, 14863-14870; e) S. Sugihara, A. Blanazs, S. P. Armes, A. J. Ryan, A. L. Lewis, *J. Am. Chem. Soc.* **2011**, *133*, 15707-15713; f) E. J. Lobb, I. Ma, N. C. Billingham, S. P. Armes, A.

L. Lewis, *J. Am. Chem. Soc.* **2001**, *123*, 7913-7914; g) S.-i. Yusa, K. Fukuda, T. Yamamoto, K. Ishihara, Y. Morishima, *Biomacromolecules* **2005**, *6*, 663-670; h) K. Ishihara, T. Ueda, N. Nakabayashi, *Polym. J.* **1990**, *22*, 355.
[5] a) Q. M. Zhang, M. J. Serpe, *Macromolecules* **2014**, *47*, 8018-8025; b) E. M. Alexandrino, S. Ritz, F. Marsico, G. Baier, V. Mailänder, K. Landfester, F. R. Wurm, *J. Mater. Chem. B* **2014**, *2*, 1298-1306.
[6] a) I. Blidi, R. Geagea, O. Coutelier, S. Mazières, F. Violleau, M. Destarac, *Polym. Chem.* **2012**, *3*, 609-612; b) L. Seiler, J. Loiseau, F. Leising, P. Boustingorry, S. Harrisson, M. Destarac, *Polym. Chem.* **2017**, *8*, 3825-3832; c) K. Markiewicz, L. Seiler, I. Misztalewska, K. Winkler, S. Harrisson, A. Wilczewska, M. Destarac, J.-D. Marty, *Polym. Chem.* **2016**, *7*, 6391-6399; d) G. Layrac, C. Gerardin, D. Tichit, S. Harrisson, M. Destarac, *Polymer* **2015**, *72*, 292-300; e) I. Blidi, O. Coutelier, M. Destarac, *J. Polym. Sci. Part A: Polym. Chem.* **2014**, *52*, 2616-2624.
[7] B. Canniccioni, S. Monge, G. David, J.-J. Robin, *Polym. Chem.* **2013**, *4*, 3676-3685.
[8] A. Hanisch, P. Yang, A. N. Kulak, L. A. Fielding, F. C. Meldrum, S. P. Armes, *Macromolecules* **2016**, *49*, 192-204.
[9] a) B. Kahr, R. W. Gurney, *Chem. Rev.* **2001**, *101*, 893-951; b) S. Mann, *Biomineralization: Principles and Concepts in Bioinorganic Materials Chemistry*, Oxford University Press: Oxford, 2001.
[10] a) C. H. Lu, L. M. Qi, H. L. Cong, X. Y. Wang, J. H. Yang, L. L. Yang, D. Y. Zhang, J. M. Ma, W. X. Cao, *Chem. Mater.* **2005**, *17*, 5218-5224; b) G. Wegner, M. M. Demir, M. Faatz, K. Gorna, R. Munoz-Espi, B. Guillemet, F. Gröhn, *Macromol. Res.* **2007**, *15*, 95-99; c) Y.-Y. Kim, K. Ganesan, P. Yang, A. N. Kulak, S. Borukhin, S. Pechook, L. Ribeiro, R. Kroeger, S. J. Eichhorn, S. P. Armes, B. Pokroy, F. C. Meldrum, *Nat. Mater.* **2011**, *10*, 890-896; d) Y. Ning, L. A. Fielding, T. S. Andrews, D. J. Growney, S. P. Armes, *Nanoscale* **2015**, *7*, 6691-6702; e) K.-R. Cho, Y.-Y. Kim, P. Yang, W. Cai, H. Pan, A. N. Kulak, J. L. Lau, P. Kulshreshtha, S. P. Armes, F. C. Meldrum, J. J. De Yoreo, *Nat. Commun.* **2016**, *7*, 10187; f) Y. Ning, D. J. Whitaker, C. J. Mable, M. J. Derry, N. J. W. Penfold, A. N. Kulak, D. C. Green, F. C. Meldrum, S. P. Armes, *Chem. Sci.* **2018**, *9*, 8396-8401; g) S. Kim, J. Choi, M. Lee, S.-H. Choi, K. Char, *Chem. Mater.* **2018**, *30*, 4048-4055; h) M. B. Al‐Handawi, P. Commins, S. Shukla, P. Didier, M. Tanaka, G. Raj, F. A. Veliz, R. Pasricha, N. F. Steinmetz, P. Naumov, *Adv. Biosyst.* **2018**, *2*, 1700176; i) A. N. Kulak, M. Semsarilar, Y.-Y. Kim, J. Ihli, L. A. Fielding, O. Cespedes, S. P. Armes, F. C. Meldrum, *Chem. Sci.* **2014**, *5*, 738-743; j) Y. Ning, L. A. Fielding, J. Nutter, A. N. Kulak, F. C. Meldrum, S. P. Armes, *Angew. Chem. Int. Ed.* **2019**, *58*, 4302-4307.
[11] a) A. G. Shtukenberg, M. D. Ward, B. Kahr, *Chem. Rev.* **2017**, *117*, 14042-14090; b) F. Nudelman, N. A. Sommerdijk, *Angew. Chem. Int. Ed.* **2012**, *51*, 6582-6596.
[12] a) R. Muñoz-Espí, G. Jeschke, I. Lieberwirth, C. M. Gómez, G. Wegner, *J. Phys. Chem. B* **2007**, *111*, 697-707; b) C. T. Hendley, L. A. Fielding, E. R. Jones, A. J. Ryan, S. P. Armes, L. A. Estroff, *J. Am. Chem. Soc.* **2018**, *140*, 7936-7945; c) Y. Ning, L. A. Fielding, K. E. B. Doncom, N. J. W. Penfold, A. N. Kulak, H. Matsuoka, S. P. Armes, *ACS Macro Lett.* **2016**, *5*, 311-315; d) Y. Ning, L. A. Fielding, L. P. D. Ratcliffe, Y.-W. Wang, F. C. Meldrum, S. P. Armes, *J. Am. Chem. Soc.* **2016**, *138*, 11734-11742.
[13] J. Ihli, P. Bots, A. Kulak, L. G. Benning, F. C. Meldrum, *Adv. Funct. Mater.* **2013**, *23*, 1965-1973.
[14] U. Wehrmeister, A. L. Soldati, D. E. Jacob, T. Haeger, W. Hofmeister, *J. Raman Spectrosc.* **2010**, *41*, 193-201.
[15] G. D. Scott, D. M. Kilgour, *J. Phys. D: Appl. Phys.* **1969**, *2*, 863.
[16] Y. Ning, L. Han, M. J. Derry, F. C. Meldrum, S. P. Armes, *J. Am. Chem. Soc.* **2019**, *141*, 2557-2567.
[17] P. de Gennes, *Macromolecules* **1980**, *13*, 1069-1075.
[18] Y. Ning, L. Han, M. Douverne, N. J. W. Penfold, M. J. Derry, F. C. Meldrum, S. P. Armes, *J. Am. Chem. Soc.* **2019**, *141*, 2481-2489.
[19] a) Y. Liu, H. Zang, L. Wang, W. Fu, W. Yuan, J. Wu, X. Jin, J. Han, C. Wu, Y. Wang, H. L. Xin, H. Chen, H. Li, *Chem. Mater.* **2016**, *28*, 7537-7543; b) Y. Liu, W. Yuan, Y. Shi, X. Chen, Y. Wang, H. Chen, H. Li, *Angew. Chem. Int. Ed.* **2014**, *53*, 4127-4131.